Analysis of Degradation Kinetics of Halide Perovskite Solar Cells Induced by Light and Heat Stress

Dhruba B. Khadka[a]*, Yasuhiro Shirai[a], Masatoshi Yanagida[a], Koichiro Uto[b], and Kenjiro Miyano[a]

[a] Photovoltaic Materials Group, Center for GREEN Research on Energy and Environmental Materials, National Institute for Materials Science (NIMS), 1-1 Namiki, Tsukuba, Ibaraki 305-0044, Japan.

[b] Research Center for Functional Materials, National Institute for Materials Science, 1-1 Namiki, Tsukuba, Ibaraki 305-0044, Japan.

Corresponding Author

*E-mail: KHADKA.B.Dhruba@nims.go.jp

ABSTRACT

The operational stability of encapsulated perovskite solar cells (PSCs) is imperative for commercialization. Here, we have investigated the degradation of PSCs with organic (PTAA) and inorganic (NiO_x) HTLs under constant illumination and thermal stress. The device parameters under 1-sun illumination were monitored over time at different temperatures; 20 to 85^{o}C. The temperature-dependent device parameters analysis showed a lower value of degradation activation energy (E_A) for the device with the PTAA (~0.274$\pm$0.05 eV) than that for the NiO_x device (~0.495$\pm$0.05 eV). This result corroborates that higher activation energy for NiO_x/HaP devices leads to superior device stability. The device degradation kinetic has been discussed by adopting the Arrhenius model with temperature and humidity prefactor correction associated with structural defects in the bulk and interfacial deterioration. Our analysis underscores the importance of the layer material's stability against humidity and thermal stress for the device stability correlating degradation activation energy and stress prefactor.

Keywords: Perovskite solar cell; Device stability; Degradation dynamics; Arrhenius model; Activation energy; humidity/thermal stress.

1. INTRODUCTION

Perovskite solar cells (PSCs) have huge potential to be fabricated with cheaper materials and production costs than conventional semiconductor solar cells [1–5]. Despite the high device efficiency, the commercialization of PSCs is impeded by long-term stability [6–9]. The device under operation accelerates the loss of power conversion efficiency (PCE). The degradation of PSCs is triggered by external stimuli, such as irradiation, heat, moisture, oxygen, electric bias, and strain [10–16]. The deterioration of the carrier transport layer (CTL) is also deleterious for device stability [17]. The degradation mechanism is stimulated with an increase in chemical kinetics at elevated temperatures, which leads to interfacial deterioration as well as delamination. The cause of operational instability of PSCs with different interface layers also largely remains elusive. Therefore, it is important to dig up the mechanistic parameters to track the degradation propagation.

An accelerating stress testing could provide a real picture of operational stability which is decisive for its commercialization [4,5]. The mean lifetime (MLT) of solar cell devices is carried out by accelerated life testing (ALT) under overstress conditions [18]. The most common stress conditions for ALT are:[19] (a) thermal stress followed by high temperature and/or temperature cycling and/or temperature gradients,(b) electrical stress with power cycling/voltage cycling/power extremes/voltage extremes [20], (c) mechanical stress with mechanical shock/stress/vibrational tests/creep-stress relaxation tests, (d) environmental stress i.e. humidity or radiation. Moreover, the ALT tests are also carried out by the combination of these tests. For example, thermal stress/humidity (typically T-85 ^{o}C/*RH*-85%) or illumination/thermal stress conditions are popularly used for the testing of the different kinds of solar cells [19–22] including PSCs [7,17,23,24]. Indeed, several reports have demonstrated a remarkable improvement in device stability introducing interfacial passivation at either HTL/perovskite or ETL/perovskite interface [25–27]. Researchers have investigated the degradation of perovskite monitoring the device parameters and discussed the different characteristic features observed in the bulk, interface, and other related optoelectronic properties [7,16,17,23,28–31]. However, there is still lacking the analysis of the degradation trend of device parameters under ALT test conditions using an analytical model that could provide insights into the degradation kinetics.

Noting that, we analyzed the trend of degradation of the device parameters of PSCs under continuous illumination driven by thermal stress. ALT was performed at various temperatures *(*20-85 ^{o}C*)* and under constant illumination of 1 sun. Illumination was provided by standard halogen lamps without blocking the UV part. The device parameters monitored at different temperatures (20 to 85 ^{o}C) with time were fitted with a linear or exponential functional model to evaluate the degradation kinetics. The mathematical analysis revealed that the poor stability of the device with PTAA is

attributed to a lower activation energy for degradation compared to the device with NiO_x. We have underlined the operational stability of PSCs with different HTLs digging into the degradation kinetics.

2. RESULTS AND DISCUSSION

To investigate the degradation kinetics, the PSCs with HTLs; PTAA, or NiO_x (Fig. S1a) were monitored under continuous illumination of one sun placing at thermal stress as mentioned in supporting information (Table S1). The device fabrication methods and characterizations details have been described in supporting information. The *J–V* characteristics of fresh devices are depicted in Fig. S1b. The PSC with the PTAA has a PCE of ~19.32% and the device with sputtered NiO_x has an efficiency of 15.60%. The detail of the fabrication method is briefly given in supporting information. The photoluminescent (PL) spectra of perovskite films (Fig. S2a) show an effective PL quenching for PTAA/HaP film that is also supported by time-resolved PL responses (Fig. S2b). It suggests that the fresh PTAA device has more effective carrier transport compared to the device with NiO_x. Our previous study revealed that the PSCs with NiO_x and PTAA have negligible interfacial mediated recombination indicating a good NiO_x/HaP or PTAA/HaP interface quality. The characteristics insights have been discussed in our earlier reports [32–34].

Furthermore, it has been documented that the PSCs with PTAA and NiO_x have different degradation rates which are attributed to the difference in the interface chemistries and their interactions with external stimuli [35,36]. The detail of degradation characteristics with the point of view of materials properties and interface quality has been documented in our earlier report [37]. In this work, we confined our study to the degradation kinetics of these devices under thermal and light stress considering the ALT model.

In thin-film solar cells, the current generated and passed through a solar cell is typically described by a simplified diode equation as given by current/voltage relation:

$$J(V)=J_L - J_0 \left(e^{\frac{q(V+JR_S)}{nK_BT}} - 1\right) - \frac{V+JR_S}{R_{SH}} \qquad (1)$$

where J(V) is the current density through the diode, and J_L is photo-induced current density, J_0 is the saturation current density, V is the external bias applied to the device, n is the ideality factor of the diode, q is the elementary charge, k_B is the Boltzmann constant, T is the absolute temperature, R_s and R_{SH} are the serial and parallel resistance of the device, respectively.

Then, the overall PCE (η) of a solar cell is given by following relations:

$$\eta = \frac{J_{SC}\times V_{OC}\times FF}{P_i} \qquad (2)$$

where V_{oc} is the open-circuit voltage, J_{sc} is the short circuit current density, FF is the fill factor and P_i is the incident solar radiation in W/m^2.

Figure 1 shows the device degradation trend at 20, 60, 85 °C, and ambient conditions (27 °C<T<35 °C) under continuous illuminations (one sun) at RH of 35-40%for t>1000 h. Photographs of the fresh devices (a, b), experimental setting (c, d), and device after thermal stress (e) are displayed in the supporting information (Fig. S3). The degradation over time of the device with PTAA (Fig. 1a) and the device with NiO_x (Fig. 1b) demonstrated a different degradation rate. This is attributed to the difference in the interface chemistries at PTAA/HaP or NiO_x/HaP and HaP bulk with external stimuli. [35,36] As given in Fig. 1c, the aged PSCs with NiO_x retained ~74.8% of PCE_0 at 20 °C, 86.7% at 60 °C, 68.7% at 85 °C, and ~90.1% under ambient condition whereas the devices with PTAA device dropped to 22.5%, 35.9%, 2.0%, and 22.6% of PCE_0, respectively. The monitored data showed that the device parameters (Figs.S4, S5) are primarily governed by the J_{sc} trend. This observation is parallel to other reports [17,35,38].

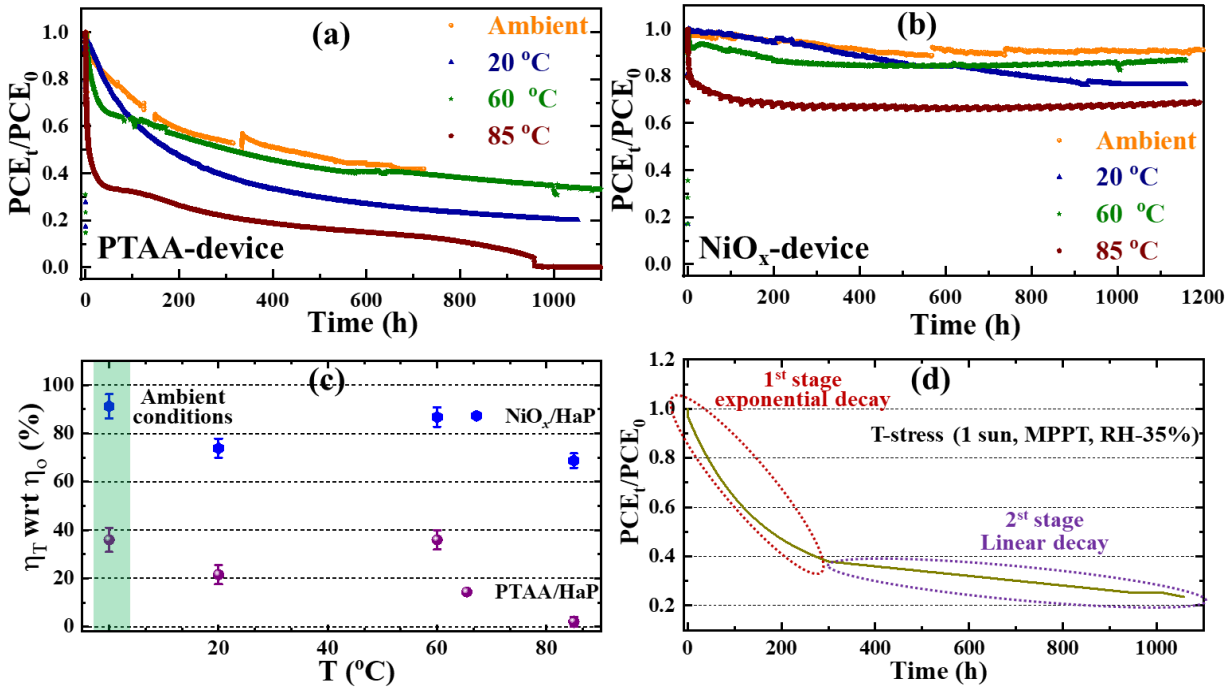

Figure 1. Long-term operational stability of the (a) PTAA/HaP and (b) NiO_x/HaP devices at different temperatures under maximum power point conditions (1 sun). (c) The relative performance of PTAA or NiO_x devices aged under different thermal stress under continuous illumination. (d) A representative schematic display of device degradation trend of PSCs under thermal stress (1 sun, MPPT) showing exponential decay at the initial stage followed by linear decay. The shaded region indicates ambient conditions.

From the device stability data, we can notice that the J_{sc} of the PTAA/HaP device dropped faster than the NiO_x/HaP device. The PSCs showed lower stability for T< RT (room temperature; 27 °C<RT<35 °C), or T>60 °C (~working at the roof temperature). Particularly, an initial steep drop

in PCE at 85 °C was observed for both devices. We also noticed a loss of fill factor in both devices. This is affected by a gradual increase of the series resistance of the devices (Fig. S6).

As depicted in schematic plot Fig. 1d, one can see the degradation trend of the PSCs with either of HTLs followed by two characteristics functional regimes. The initial stage of degradation shows the exponential decay which is followed by a linear decay. Indeed, the rate of exponential or linear decay is influenced by the carrier transport layer used in the device configuration. This observation is parallel to the degradation behavior reported by others [7,39]. These trends are the consequence of collective effects of the partial degradation of CTL, defect induced in HaP bulk by crystal phase transformation, and CTL/HaP interface of either side under higher thermal stress and illumination [24,37,39,40].

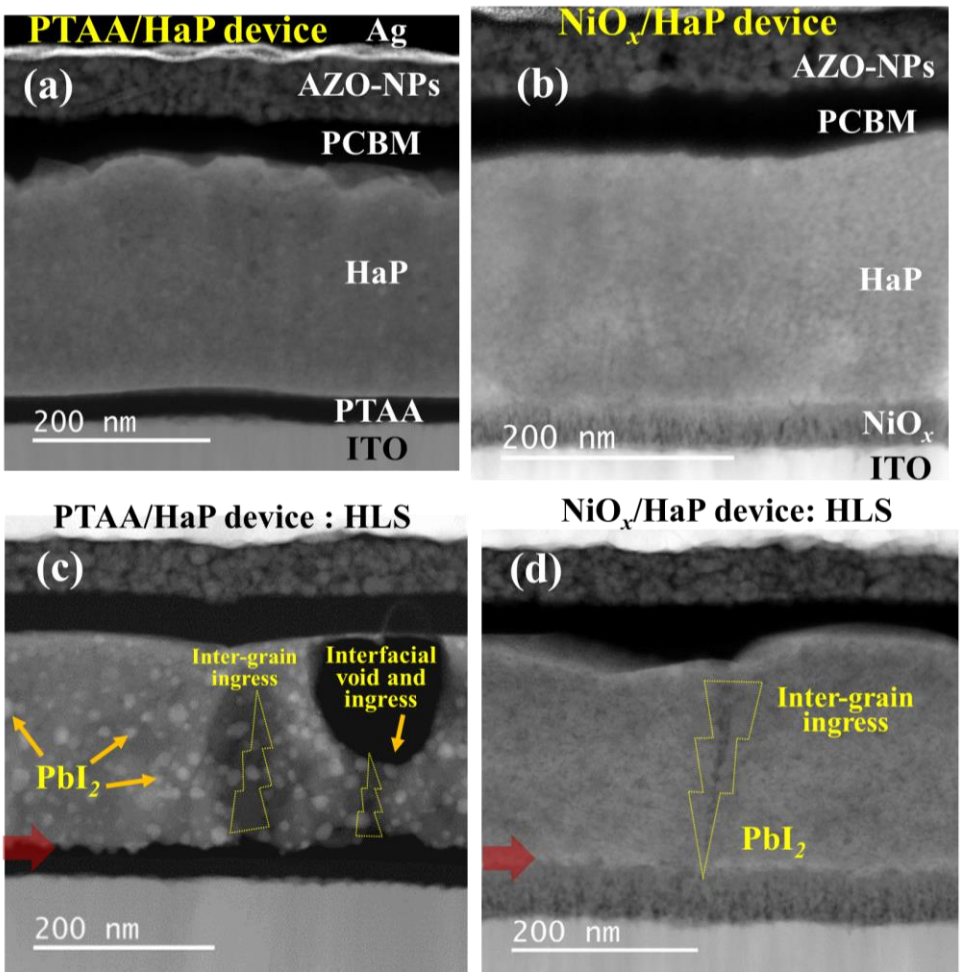

Figure 2. STEM cross-sectional images of fresh (a, b) and aged (light and thermal stress (1000 hr- 60 ^{o}C)) (c, d) of PSCs with PTAA and NiO_x as HTL. ➡ indicates HTL/HaP interface.

Figure 2 shows STEM cross-sectional images of PSCs with PTAA and NiOx as HTLs of fresh and aged under heat and light stress (HLS). It reveals a clear picture of the mode of degradation of PSCs with different HTLs that is parallel to the device degradation for respective devices (Fig. 1). The PTAA device shows bulk degradation with the formation of small crystallites of PbI_2 at the PTAA or

PCBM/HaP interfaces and voids. While there are no obvious voids and PbI_2 crystallites formed in the NiO_x device indicating relatively intact bulk and interface.

To understand the surface free energy on the film surface, we collected the water contact angle on fresh and aged PTAA and NiO_x films. As given in supporting information (Fig. S7), the water contact angles on the surface of the fresh PTAA (~83.5^o) shows a lower value on the PTAA film aged under HLS (54.2^o). While that for the NiO_x films remains almost unchanged under aging (~53.4^o on the fresh surface to 52.1^o on the aged surface). These results corroborate that the PTAA film loses its hydrophobicity under HTL aging which could deteriorate the PTAA/HaP interface quality under HLS. It is reported that the stability of PSCs with polymer-based HTL is improved using composite layers (PEDOT: PSS/PTAA)[41]. E. Kymakis and co-workers have documented a few critical limitations of a polymer-based HTL in planar inverted perovskite solar cells.[35] It is noted that a polymer-HTL (PTAA) film absorbs a high-energy photon under illumination. It results in stretching of hydrocarbon ring and polymer chain in PTAA molecules. This leads to partial decomposition of the cyclic structure under a longer aging stress environment. This claim is also parallel to the water contact angle results on aged PTAA surface (Fig. S7). Being less moisture resistive nature of PTAA, it is more prone at lower temperatures which partly triggers bulk degradation and interface corrosion. A detailed discussion on the degradation of materials and optoelectronic characteristics of PSCs can be found in our previous report [37].

In this study, we have monitored only the change of the device parameters due to degradation over time. These changes in the device parameters have been analyzed by a mathematical model accounting for temperature and moisture effect. The lifetime of the device has been predicted. In this work, since the temperature of the device under ambient conditions was not controlled (27 °C<RT<35 °C), we did not use the corresponding data for further analysis using the ALT model hereafter.

2.1 Accelerated degradation testing model

The degradation kinetics can be analyzed by ALT models [42]. The Arrhenius Equation, the Eyring Equation, and the Power Law are widely adopted for analyzing the degradation of electronic components [43]. The Arrhenius model deals with the most fundamental mathematical model for the analysis of optoelectronic device characteristics. The degradation constant for this model is given by:

$$k = Ae^{\left(-\frac{E_A}{K_B T}\right)} \quad (3)$$

Here, E_A- the activation energy, k_B- the Boltzmann constant 8.62×10^{-5} eVK^{-1}, T- the temperature in Kelvin and A - a constant dependent on the degradation mechanisms and the experimental conditions. It collectively explains the device deterioration consisting of activation energy of degradation (E_A), which influences the kinetics of device degradation. The characteristics values are mainly affected by

material properties such as the trapping behavior of electrical carriers or structural and chemical changes of different layers of the device architecture. The Arrhenius model primarily explains the kinetics of the temperature-dependent process.

Moreover, to account for the multiple stress factors, the Eyring model, a complex form of the Arrhenius model is used [44]. The external stress factors for the solar cell or photodetector degradation could be the externally applied bias, the light intensity, humidity, etc. In the Eyring model, the degradation factor is defined by,

$$K_{deg} = AT^{\alpha} \exp\left[-\frac{-E_A}{K_B T} + (B + \frac{C}{T})S_1\right] \quad (4)$$

where, the terms S_1, α, B, and C, are additive coefficients to the Arrhenius part in the exponential term, are related to stress characteristics. The terms; k_B and T are as noted above. Indeed, the Eyring model is dedicated to describing more complex degradation behavior. Note that as we controlled the experimental methods to prevent additional stress factors and if α is negligible, the Eyring equation is equivalent to the Arrhenius equation.

Similarly, the third ALT model is the inverse power model. It is used to study the degradation of electronic or dielectric devices. The degradation constant for this model is given by

$$k_{deg} = AV^{\gamma} \quad (5)$$

here, V is the electrical stress (for instance, applied voltage or current). A and γ are product-specific parameters related to the component materials. This model is more relevant for organic materials related to optoelectronic products (organic light-emitting diodes, transistors, or photodetectors) under constant temperature stressed by different bias or current levels rather than PV devices.

In this work, we monitored the device parameters varying thermal stress under constant illumination and humidity. Therefore, we used the Arrhenius model for the analysis of device characteristics with aging.

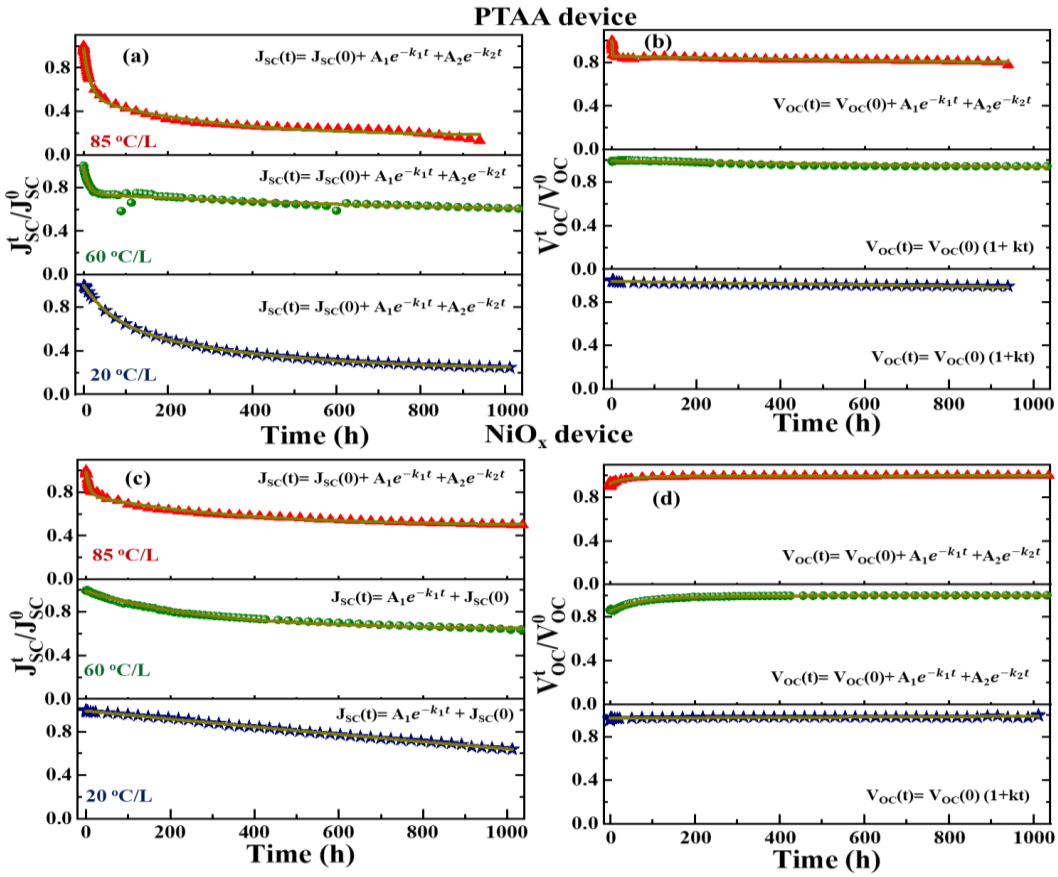

Figure 3. The trend of degradation of device parameters **(**J_{SC} and V_{OC}**)** for PSCs with PTAA (a, b) or NiO_x (c, d) under continuous illumination for more than 1000 h at 20, 60, and 85 °C. The lines represent a nonlinear fitting of respective parameters. Note that few scattered data at the beginning and the endpoint have been omitted for better fitting. The fitting functions (linear or exponential) are given on the respective plot.

2.2 Determination of the degradation kinetics

To analyze the degradation kinetic overtime under thermal stress, we have performed the fitting of the device parameters with time considering a mathematical model.

The degradation trend of PCE of the device is given by linear model;

$$\eta(t) = \eta_0 (1 - k_{deg} t) \quad (6)$$

And exponential model

$$\eta(t) = \eta_0 e^{-K_{deg} t} \quad (7)$$

Where, $\eta(t)$ is the PCE of the device at a time (t) under thermal stress, η_0 is the PCE of the device at time t=0. From Equation (2), we can express the device parameters comprising η (V_{oc}, J_{SC}, and FF) in the linear or exponential model.

We fitted the device parameters using either of the mathematical models given by equations 6 and 7 as shown in Fig. 3. The J_{sc} (t) trends are described by the exponential model whereas the trends of FF and V_{OC} are explained by a linear model. The FF(t) and V_{OC}(t) have a slow degradation rate. The fitting equations and parameters are given in the supporting information (Tables. S2, 3). The fitted parameters for J_{SC} show a positive exponential constant in the decay function. It suggests an exponential decay trend for both devices. On the other hand, the fitted parameters for V_{OC} of the device with PTAA result in a negative slope in the linear equation and a positive exponential constant for the exponential decay equation, which suggests a loss of V_{OC} with aging. However, the fitted parameters for V_{OC} of the NiO_x device show a positive slope in linear fitting and negative exponential constant for fitting of exponential decay equation (Table S3). These results corroborate an increase in V_{OC} with thermal stress in the device with NiO_x. Thus, a collective parameter trend drives the deterioration of device performance with aging. Particularly, the J_{sc} drives the degradation of PCE with aging. Besides that, the R_s values with aging (Figs. S6) at 20 and 60 ^oC are well fitted with a linear model.

$$R_s(t)= R_s(0)(1+kt)] \quad (8)$$

While those data at 85^oC were described by exponential grow model is given by

$$R_s(t)=R_s(0)+ A_1e^{k_1t} +A_2e^{k_2t} \quad (9)$$

Each notation has a corresponding meaning as mentioned in the previous equation. The R_s of the PTAA/HaP device demonstrated a higher value compared to the NiO_x*/HaP* device. The fitted parameters are tabulated in supporting information (Table S4). The slope of linear fitting (e.g., 60 ^oC) shows that the rate of increase in R_s of the device with PTAA (~0.079 Ω/hr) is more than one order higher compared to the device with NiO_x (~0.0032 Ω/hr). The R_s for the device with PTAA at 85 ^oC showed two-phase exponentials grow with positive fitting parameters while that for the device with NiO_x fitted with the negative/positive value indicates a slow increase in R_s at a higher temperature. It substantiates that the device with PTAA is highly vulnerable to higher thermal stress. This is attributed to the partial decomposition of the PTAA layer under HLS [35] and the degradation of the bulk layer driven by interface deterioration [37].

We evaluated the trajectory of degradation kinetics for each aging stress condition by fitting device parameters. Among the temperature-accelerated device parameters, the J_{SC} degradation trend is parallel to the loss of PCE. Therefore, we analyzed the J_{sc} trend at different thermal stress to calculate the degradation activation energy [18]. The degradation constant with temperature extracted from Fig. 3 gives an Arrhenius-type dependent (Figs. 4a,b). This observation is analogous to that reported for organic [18] and Si-based solar cells. [20] The Arrhenius type degradation model (equation (1)) was applied for the evaluation of the temperature dependence. The activation energy of the device with

NiO_x for degradation (0.495±0.02 eV) is higher than that of the PTAA device (0.274±0.02 eV). It indicates that the PTAA device, with lower activation energy, degrades faster. As summarized in Table S5, the estimated values of E_A for our devices are lower than Si, CIGS, or CdTe- based devices which are well-known for stable device performance with much higher MLT. It implicates that the value of E_A is directly proportional to the MLT of PSCs. We believed that the difference in E_A for the PSCs with PTAA and NiO_x is attributed to the structural defect in perovskite, interfacial deterioration of HTL/HaP, and HTL under HLS [24]. It is also supported by the degradation trajectory of respective devices. A lower value of E_A for the PSC with PTAA could have stemmed from structural defect induced from thermal stress [24,40] and the partial deterioration of the PTAA film due to absorption of a high-energy photon (Fig. S8) under illumination.[35] While higher activation energy for the device with the NiO_x is analogous to the relatively stable device due to the robust nature of NiO_x which results in a comparatively stable interface and immune to ionic diffusion for the perovskite bulk [45].

To get more insights into the degradation kinetics, the acceleration factor for the individual temperatures was determined under the assumption of an Arrhenius model according to (8):

$$K=\frac{k_{deg}(T_H)}{k_{deg}(T_L)}= \exp\left[\frac{E_A}{K_B}\left(\frac{1}{T_L}-\frac{1}{T_H}\right)\right] \quad (8)$$

where T_L and T_H correspond to low and high temperatures (reference temperature). In our analysis, we considered T_H =85 ^oC (standard temperature for reliability test). Note that a higher value of acceleration factor (K) denotes better device stability.

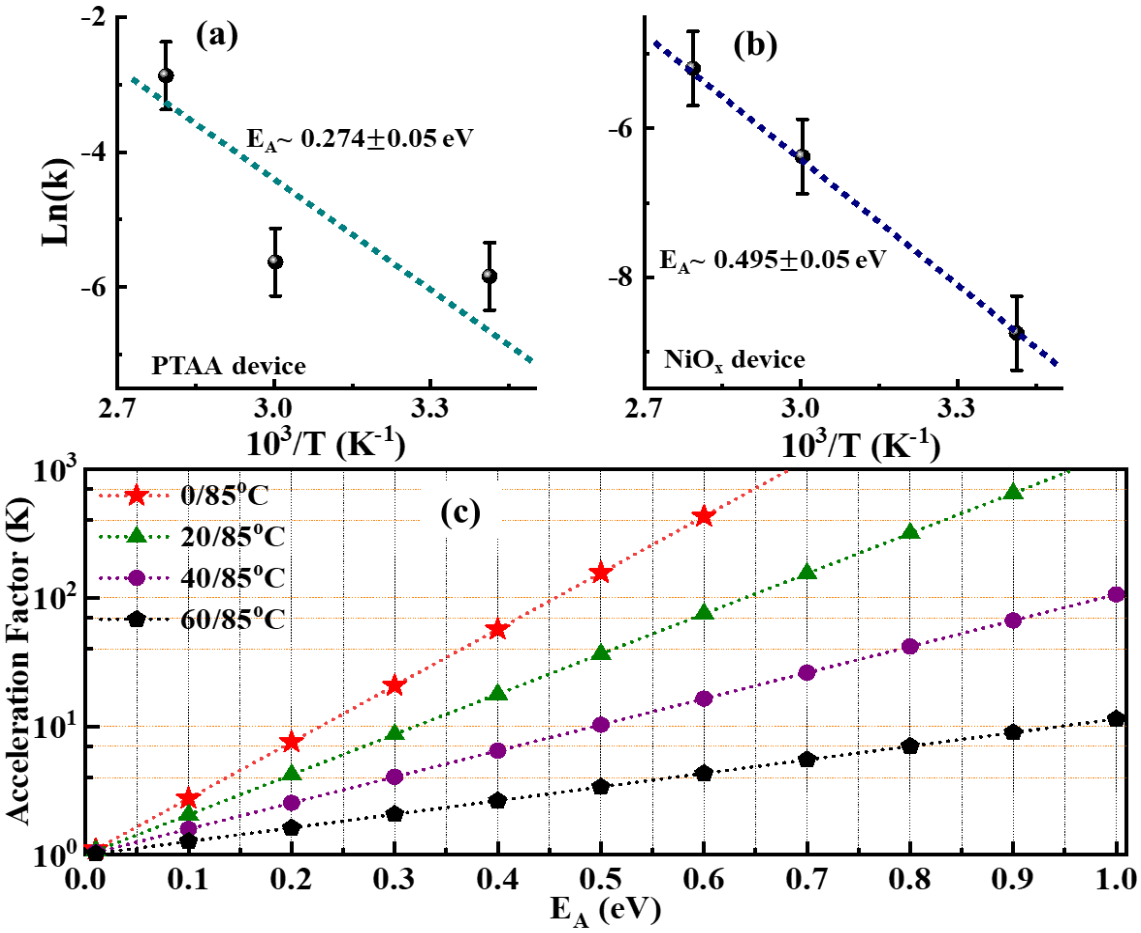

Figure 4. The degradation activation energy of PSCs with (a) the PTAA and (b) NiO_x is estimated by analyzing the trend of device parameters (J_{SC}). The estimation of acceleration factor of the device considering prefactor with the varying working low temperatures (T_L) with reference to the standard test temperature (T_H=85 °C) adopting the Arrhenius equation (8).

We have calculated the acceleration factor of degradation using equation (8) at working temperature (T_L) (T_L= 0 °C (winter), 20 °C (~below room temperature), 32 °C (~ ambient working temperature), and 60 °C (~working at the roof temperature) (Fig. 4c) with respect to 85 °C. This result shows a higher acceleration factor at a lower working temperature. This means the MLT of the device is longer at a lower working temperature (T<85 °C). Unlike the Arrhenius estimation, the experimental device data showed poor stability for T<20 °C. It is to be noted that the environmental stress (temperature and ambient humidity) induces the defects such as structural defect and deterioration of interface or bulk layer used in device structures[37,39,40] which could be the main factors for the anomalous trend (Fig. 1c).

At first, we introduced an additional prefactor to account for the deterioration of the materials due to thermal stress. We modified the Arrhenius equation (8) by adding a temperature-driven prefactor defined by two models.

Model-1 is defined by adding linear temperature prefactor,

$$K = A \exp\left[\frac{E_A}{K_B}\left(\frac{1}{T_L} - \frac{1}{T_H}\right)\right] \times \left(\frac{T_L}{T_H}\right)^{\alpha} \quad (9)$$

and model-2 is defined by adding exponential temperature prefactor,

$$K = A \exp\left[\frac{E_A}{K_B}\left(\frac{1}{T_L} - \frac{1}{T_H}\right)\right] \times \exp\left(\frac{T_L}{T_H}\right)^{-\alpha} \quad (10)$$

Here, the temperature prefactor (α) accounts for the degree of material deterioration with thermal stress. The acceleration factors with temperature prefactor are given by model-1 and 2 (equations-9 and 10) (Figs. 5a, b; S9a-c). The model-2 consisting of an exponential prefactor shows suppression of the degradation factor by one order value while the linear prefactor (model-1) has minimal effect. The calculation (Figs. 5c, d) shows a higher loss in the MLT of the device with an increase of α which is attributed to the degree of material degradation under thermal stress. One can see the drop of MLT at a lower temperature regime for model-1while that for model-2 shows a significant drop at all temperature ranges. With these observations, it is proposed that the PTAA device could have been driven by a temperature prefactor with an exponential function (exponent value α<2.5), and the device with NiO_x -HTL follows the linear function (exponent value α<2.5) at a higher temperature regime. This means the device with NiO_x protects the degradation of perovskite bulk and interfaces by deaccelerating the temperature effect. Moreover, it has been documented that the structural transformation of $MAPbI_3$ occurs as a function of temperature, thermal stress time, or halide additive [40,46,47]. It is suggested that more structural defects are formed under thermal stress. Since the structural defects are more sensitive to external stimuli, it drives degradation trend by deteriorating material properties that could be accounted by prefactor coefficient as shown in Figs. 5a-d. Furthermore, although the lower stability at a higher temperature regime (T>35 ^{o}C) can be partially explained by the characteristics feature of these models, this mathematical formulation does not support the poor device stability at lower temperature regime 20 ^{o}C (T < RT).

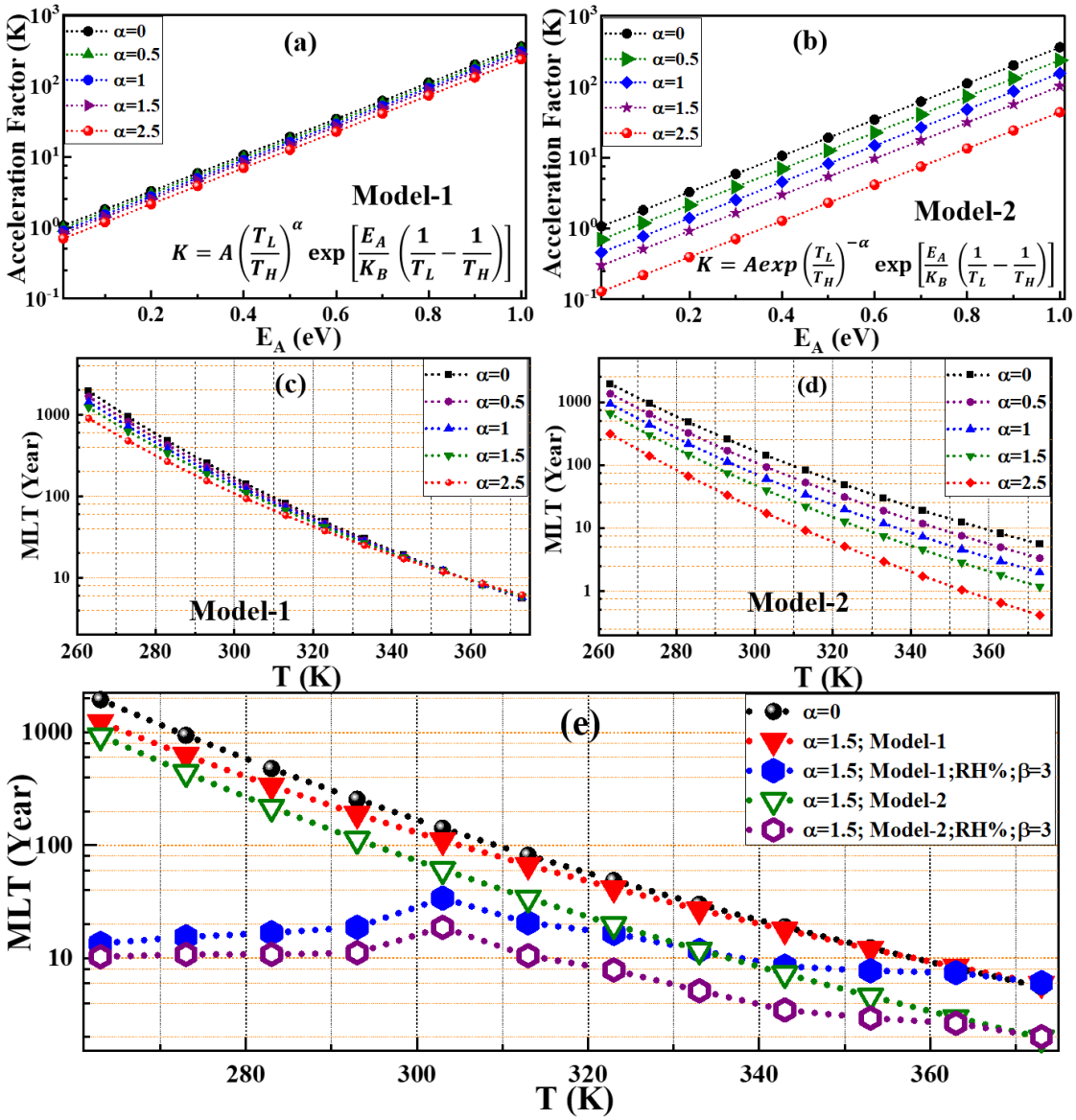

Figure 5. The acceleration factor and activation energy (E_A) introducing temperature prefactor in Arrhenius equation given by (a) model-1 (Equation (9)) and (b) model-2 (equation (10)) at working temperature T_L=30 ^oC with reference to the standard test temperature (T_H=85 ^oC) by varying material characteristics with thermal stress given by prefactor coefficient (α). The plots; (c-f) give mean lifetime (MLT) accounting model-1 and model-2 corresponding to (a, b) with the varying working temperatures (T_L) with reference to the standard test temperature (T_H=85 ^oC). For MLT calculation, we have considered that that device (the device with NiO_x) retains ~70% of its performance by 1000 hours. The simulation of acceleration factor with consideration of humidity effect (e). Note that mean lifetime (MLT) is given by $MLT(T)= MLT_H \times K$, where MLT_H- is the mean lifetime of PSCs at TH=85 ^oC.

To explain the degradation trend at lower temperatures (T<RT), we redefined the model with temperature prefactor adding the humidity prefactor. We accounted for the humidity stress ramping with thermal stress which could further accelerate the material deterioration through the structural defects.[40] As the device stability data are collected in an enclosed testing system, there is also the possibility of variation of relative humidity with temperature stress. In the enclosed system, the humidity of ~35-40% at room temperature can vary from RH>75% at lower temperatures (T<20 ^{o}C) to RH>28% at high temperature (T~85^{o}C). As we performed the device test under thermal stress by lowering the temperature, the enclosed ambient moisturizes which affects the perovskite device performance.[48] It has also been documented that there is a higher possibility of ingress of moisture even though the edge of the device is sealed.[10] Thus, taking account of humidity effect, we adopted the Hallberg-Peck acceleration model, the equations (9) and (10) with humidity factor can be written as;[43]

$$K = A \exp\left[\frac{E_A}{K_B}\left(\frac{1}{T_L} - \frac{1}{T_H}\right)\right] \times \left(\frac{T_L}{T_H}\right)^{\alpha} \times \left(\frac{RH_L}{RH_H}\right)^{-\beta} \quad (11)$$

$$K = A \exp\left[\frac{E_A}{K_B}\left(\frac{1}{T_L} - \frac{1}{T_H}\right)\right] \times \exp\left(\frac{T_L}{T_H}\right)^{-\alpha} \times \left(\frac{RH_L}{RH_H}\right)^{-\beta} \quad (12)$$

Here, the value of β signifies the degree of material degradation at lower temperatures with moisture ingress. Figure 5 shows the estimation of MLT of the device at different working temperatures (T_L) with the reference of the standard test temperature (T_H=85 ^{o}C). Note that the lower prefactor value shows a weak effect on device deterioration which corresponds to moisture resistive material properties. The plots of MLT with varying humidity prefactor (Figs. S9f, g) indicate that lower stability can be explained by adding the humidity prefactor. Each model explains the degradation of PSCs at a lower temperature for β<3. The device with PTAA has poor stability at lower working temperatures because the PTAA layer is less moisture resistive compared to NiO_x. Those devices will further deteriorate under additional light stress which explains a higher rate of loss of the PCE of PSC with PTAA.

For example, if the PSC with NiO_x retains device performance of 70% at 85 ^{o}C at 25% RH for 1000 hours which has E_A~0.5 eV. The Arrhenius model with temperature prefactor suggests that the device will retain its efficiency for 2.7, 11.2, and 18.6 times longer at a working temperature, of 60, 30, and 20 ^{o}C for temperature prefactor α=1.5 in the linear model. The MLT will be dropped to 1.2, 3.4, and 1.87 times at working temperatures of 60, 30, and 20 (>RT) ^{o}C for temperature prefactor α=1.5 and humidity prefactor β=3 for linear prefactor model. We also notice a faster decrease in MLT for the exponential prefactor model as indicated by a lower degradation factor with respect to T_H=85 ^{o}C. Collectively, it tells us the humidity prefactor could be the dominant factor for lowering the MTL even

for the encapsulated device at lower working temperatures. This implicates the importance of heat and moisture resistive materials as well as inert packing to preserve the device's lifetime.

In our analysis, we found a tentative trend with $\alpha \leq 1.5$ and $\beta \leq 3$ as displayed in Fig. 5e. It observed that the exponent constants for temperature or humidity prefactor are sensitive which is significantly influenced by the structural defect of perovskite, partial deformation of CTL, and interface quality against the thermal and moisture stress. This work underlines the importance of device structure in thermal stress in enclosed testing ambient.

3. CONCLUSIONS

We have explored the temperature accelerated degradation of PSCs with different interface layers under constant illumination. The device with NiO_x showed superior stability compared to the device with PTAA. The degradation trend for both devices is governed by an exponential decay of J_{SC} while other parameters (V_{OC} and FF) follow the linear trend. We observed an Arrhenius type dependence of the degradation constant with temperature. The analysis of the degradation trend of device parameters demonstrated higher activation energy for PSCs with NiO_x (~495 ± 50 meV) compared to that for the device with PTAA E_A of ~274 ± 50 meV indicating the interfacial effect on degradation potentials. Our analysis indicates that the device degradation kinetics of PSCs can be described by the Arrhenius model with the introduction of temperature and humidity prefactor especially at lower working temperature (T<RT) while device stability at higher working temperature (T>30 ^{o}C) follows the regular trend with temperature prefactor. This work suggests that the degradation trend of PSCs can be deaccelerated by stabilizing the structural phase of HaP under thermal stress followed by tailoring the interfacial layer with higher activation energy.

SUPPLEMENTARY MATERIALS

Experimental section, device configuration/J-V characteristics, device photograph and degradation monitoring, aging conditions, device aging parameters, fitting parameters, contact angle data, absorption spectra, table of activation energy of different solar cells, theoretical fitting of degradation characteristics.

CONFLICTS OF INTEREST

There are no conflicts to declare.

ACKNOWLEDGEMENTS

This work was supported by Yazaki Memorial Foundation for Science and Technology.

REFERENCES

[1] A. Kojima, K. Teshima, Y. Shirai, T. Miyasaka, Organometal Halide Perovskites as Visible-Light Sensitizers for Photovoltaic Cells, J. Am. Chem. Soc. 131 (2009) 6050. https://doi.org/10.1021/ja809598r.

[2] M.A. Green, E.D. Dunlop, J. Hohl-Ebinger, M. Yoshita, N. Kopidakis, X. Hao, Solar cell efficiency tables (version 56), Prog. Photovoltaics Res. Appl. 28 (2020) 629–638. https://doi.org/10.1002/pip.3303.

[3] T.M. Brenner, D.A. Egger, L. Kronik, G. Hodes, D. Cahen, Hybrid organic-inorganic perovskites: low-cost semiconductors with intriguing charge-transport properties, Nat. Rev. Mater. 1 (2016) 15007. https://doi.org/10.1038/natrevmats.2015.7.

[4] M. Cai, Y. Wu, H. Chen, X. Yang, Y. Qiang, L. Han, Cost-Performance Analysis of Perovskite Solar Modules, Adv. Sci. 4 (2017) 1600269. https://doi.org/10.1002/advs.201600269.

[5] R. Vidal, J. Alberola-Borràs, N. Sánchez-Pantoja, I. Mora-Seró, Comparison of Perovskite Solar Cells with other Photovoltaics Technologies from the Point of View of Life Cycle Assessment, Adv. Energy Sustain. Res. 2 (2021) 2000088. https://doi.org/10.1002/aesr.202000088.

[6] M. Saliba, M. Stolterfoht, C.M. Wolff, D. Neher, A. Abate, Measuring Aging Stability of Perovskite Solar Cells, Joule. 2 (2018) 1019–1024. https://doi.org/10.1016/j.joule.2018.05.005.

[7] K. Domanski, E.A. Alharbi, A. Hagfeldt, M. Grätzel, W. Tress, Systematic investigation of the impact of operating conditions on the degradation behaviour of perovskite solar cells, Nat. Energy. 3 (2018) 61–67. https://doi.org/10.1038/s41560-017-0060-5.

[8] W. Tress, K. Domanski, B. Carlsen, A. Agarwalla, E.A. Alharbi, M. Graetzel, A. Hagfeldt, Performance of perovskite solar cells under simulated temperature-illumination real-world operating conditions, Nat. Energy. 4 (2019) 568–574. https://doi.org/10.1038/s41560-019-0400-8.

[9] D.B. Khadka, Y. Shirai, M. Yanagida, K. Miyano, Pseudohalide Functional Additives in Tin

Halide Perovskite for Efficient and Stable Pb-Free Perovskite Solar Cells, ACS Appl. Energy Mater. 4 (2021) 12819–12826. https://doi.org/10.1021/acsaem.1c02496.

[10] Y. Han, S. Meyer, Y. Dkhissi, K. Weber, J.M. Pringle, U. Bach, L. Spiccia, Y.-B. Cheng, Degradation observations of encapsulated planar CH3NH3PbI3 perovskite solar cells at high temperatures and humidity, J. Mater. Chem. A. 3 (2015) 8139–8147. https://doi.org/10.1039/C5TA00358J.

[11] S.-W. Lee, S. Kim, S. Bae, K. Cho, T. Chung, L.E. Mundt, S. Lee, S. Park, H. Park, M.C. Schubert, S.W. Glunz, Y. Ko, Y. Jun, Y. Kang, H. Lee, D. Kim, UV Degradation and Recovery of Perovskite Solar Cells, Sci. Rep. 6 (2016) 38150. https://doi.org/10.1038/srep38150.

[12] D. Wang, M. Wright, N.K. Elumalai, A. Uddin, Stability of perovskite solar cells, Sol. Energy Mater. Sol. Cells. 147 (2016) 255–275. https://doi.org/10.1016/j.solmat.2015.12.025.

[13] J. Yang, B.D. Siempelkamp, D. Liu, T.L. Kelly, Investigation of CH3NH3PbI3 Degradation Rates and Mechanisms in Controlled Humidity Environments Using in Situ Techniques, ACS Nano. 9 (2015) 1955–1963. https://doi.org/10.1021/nn506864k.

[14] S. Bae, S. Kim, S.W. Lee, K.J. Cho, S. Park, S. Lee, Y. Kang, H.S. Lee, D. Kim, Electric-Field-Induced Degradation of Methylammonium Lead Iodide Perovskite Solar Cells, J. Phys. Chem. Lett. 7 (2016) 3091–3096. https://doi.org/10.1021/acs.jpclett.6b01176.

[15] J. Zhao, Y. Deng, H. Wei, X. Zheng, Z. Yu, Y. Shao, J.E. Shield, J. Huang, Strained hybrid perovskite thin films and their impact on the intrinsic stability of perovskite solar cells, Sci. Adv. 3 (2017) eaao5616. https://doi.org/10.1126/sciadv.aao5616.

[16] D.B. Khadka, Y. Shirai, M. Yanagida, K. Miyano, Degradation of encapsulated perovskite solar cells driven by deep trap states and interfacial deterioration, J. Mater. Chem. C. 6 (2018) 162–170. https://doi.org/10.1039/C7TC03733C.

[17] T.H. Schloemer, J.A. Raiford, T.S. Gehan, T. Moot, S. Nanayakkara, S.P. Harvey, R.C. Bramante, S. Dunfield, A.E. Louks, A.E. Maughan, L. Bliss, M.D. McGehee, M.F.A.M. van Hest, M.O. Reese, S.F. Bent, J.J. Berry, J.M. Luther, A. Sellinger, The Molybdenum Oxide Interface Limits the High-Temperature Operational Stability of Unencapsulated Perovskite Solar Cells, ACS Energy Lett. 5 (2020) 2349–2360. https://doi.org/10.1021/acsenergylett.0c01023.

[18] S. Schuller, P. Schilinsky, J. Hauch, C.J. Brabec, Determination of the degradation constant of bulk heterojunction solar cells by accelerated lifetime measurements, Appl. Phys. A. 79 (2004) 37–40. https://doi.org/10.1007/s00339-003-2499-4.

[19] T. Walter, Reliability Issues of CIGS-Based Thin Film Solar Cells, in: Semicond. Semimetals, 2015: pp. 111–150. https://doi.org/10.1016/bs.semsem.2015.05.001.

[20] M. Bähr, K. Lauer, Analysis of Activation Energies and Decay-time Constants of Potential-induced Degraded Crystalline Silicon Solar Cells, Energy Procedia. 77 (2015) 2–7. https://doi.org/10.1016/j.egypro.2015.07.002.

[21] D.S. Albin, Accelerated stress testing and diagnostic analysis of degradation in CdTe solar cells, in: N.G. Dhere (Ed.), Reliab. Photovolt. Cells, Modul. Components, Syst., 2008: p. 70480N. https://doi.org/10.1117/12.795360.

[22] J. Nishinaga, Y. Kamikawa, S. Ishizuka, H.L. Guthrey, H. Shibata, S. Niki, Significance of metastable acceptors in Cu(In,Ga)Se 2 solar cells in accelerated lifetime testing, Jpn. J. Appl. Phys. 57 (2018) 092301. https://doi.org/10.7567/JJAP.57.092301.

[23] S. Ma, Y. Bai, H. Wang, H. Zai, J. Wu, L. Li, S. Xiang, N. Liu, L. Liu, C. Zhu, G. Liu, X. Niu, H. Chen, H. Zhou, Y. Li, Q. Chen, 1000 h Operational Lifetime Perovskite Solar Cells by Ambient Melting Encapsulation, Adv. Energy Mater. 10 (2020) 1902472. https://doi.org/10.1002/aenm.201902472.

[24] J. Lim, M. Kim, H.H. Park, H. Jung, S. Lim, X. Hao, E. Choi, S. Park, M. Lee, Z. Liu, M.A. Green, J. Seo, J. Park, J.S. Yun, Kinetics of light-induced degradation in semi-transparent perovskite solar cells, Sol. Energy Mater. Sol. Cells. 219 (2021) 110776. https://doi.org/10.1016/j.solmat.2020.110776.

[25] X. Hu, H. Wang, Y. Ying, M. Wang, C. Zhang, Y. Ding, H. Li, W. Li, S. Zhao, Z. Zang, Methylammonium chloride as an interface modificator for planar-structure perovskite solar cells with a high open circuit voltage of 1.19V, J. Power Sources. 480 (2020) 229073. https://doi.org/10.1016/j.jpowsour.2020.229073.

[26] M. Wang, W. Li, H. Wang, K. Yang, X. Hu, K. Sun, S. Lu, Z. Zang, Small Molecule Modulator at the Interface for Efficient Perovskite Solar Cells with High Short-Circuit Current Density and Hysteresis Free, Adv. Electron. Mater. 6 (2020) 2000604. https://doi.org/10.1002/aelm.202000604.

[27] M.J. Jeong, K.M. Yeom, S.J. Kim, E.H. Jung, J.H. Noh, Spontaneous interface engineering for dopant-free poly(3-hexylthiophene) perovskite solar cells with efficiency over 24%, Energy Environ. Sci. 14 (2021) 2419–2428. https://doi.org/10.1039/D0EE03312J.

[28] T. Yang, N.J. Jeon, H. Shin, S.S. Shin, Y.Y. Kim, J. Seo, Achieving Long-Term Operational Stability of Perovskite Solar Cells with a Stabilized Efficiency Exceeding 20% after 1000 h, Adv. Sci. 6 (2019) 1900528. https://doi.org/10.1002/advs.201900528.

[29] H.J. Jung, D. Kim, S. Kim, J. Park, V.P. Dravid, B. Shin, Stability of Halide Perovskite Solar Cell Devices: In Situ Observation of Oxygen Diffusion under Biasing, Adv. Mater. 30 (2018) 1802769. https://doi.org/10.1002/adma.201802769.

[30] D. Bryant, N. Aristidou, S. Pont, I. Sanchez-Molina, T. Chotchunangatchaval, S. Wheeler, J.R. Durrant, S.A. Haque, Light and oxygen induced degradation limits the operational stability of methylammonium lead triiodide perovskite solar cells, Energy Environ. Sci. 9 (2016) 1655–1660. https://doi.org/10.1039/C6EE00409A.

[31] T. Duong, Y. Wu, H. Shen, J. Peng, S. Zhao, N. Wu, M. Lockrey, T. White, K. Weber, K. Catchpole, Light and elevated temperature induced degradation (LeTID) in perovskite solar cells and development of stable semi-transparent cells, Sol. Energy Mater. Sol. Cells. 188 (2018) 27–36. https://doi.org/10.1016/j.solmat.2018.08.017.

[32] D.B. Khadka, Y. Shirai, M. Yanagida, K. Miyano, Unraveling the Impacts Induced by Organic and Inorganic Hole Transport Layers in Inverted Halide Perovskite Solar Cells, ACS Appl. Mater. Interfaces. 11 (2019) 7055–7065. https://doi.org/10.1021/acsami.8b20924.

[33] D.B. Khadka, Y. Shirai, M. Yanagida, T. Masuda, K. Miyano, Enhancement in efficiency and optoelectronic quality of perovskite thin films annealed in MACl vapor, Sustain. Energy Fuels. 1 (2017) 755–766. https://doi.org/10.1039/C7SE00033B.

[34] D.B. Khadka, Y. Shirai, M. Yanagida, J.W. Ryan, K. Miyano, Exploring the effects of interfacial carrier transport layers on device performance and optoelectronic properties of planar perovskite solar cells, J. Mater. Chem. C. 5 (2017) 8819–8827. https://doi.org/10.1039/C7TC02822A.

[35] M. Petrović, T. Maksudov, A. Panagiotopoulos, E. Serpetzoglou, I. Konidakis, M.M. Stylianakis, E. Stratakis, E. Kymakis, Limitations of a polymer-based hole transporting layer for application in planar inverted perovskite solar cells, Nanoscale Adv. 1 (2019) 3107–3118.

https://doi.org/10.1039/C9NA00246D.

[36] S. Thampy, B. Zhang, K.-H. Hong, K. Cho, J.W.P. Hsu, Altered Stability and Degradation Pathway of CH3NH3PbI3 in Contact with Metal Oxide, ACS Energy Lett. 5 (2020) 1147–1152. https://doi.org/10.1021/acsenergylett.0c00041.

[37] D.B. Khadka, Y. Shirai, M. Yanagida, K. Miyano, Insights into Accelerated Degradation of Perovskite Solar Cells under Continuous Illumination Driven by Thermal Stress and Interfacial Junction, ACS Appl. Energy Mater. 4 (2021) 11121–11132. https://doi.org/10.1021/acsaem.1c02037.

[38] F. Fu, S. Pisoni, Q. Jeangros, J. Sastre-Pellicer, M. Kawecki, A. Paracchino, T. Moser, J. Werner, C. Andres, L. Duchêne, P. Fiala, M. Rawlence, S. Nicolay, C. Ballif, A.N. Tiwari, S. Buecheler, I 2 vapor-induced degradation of formamidinium lead iodide based perovskite solar cells under heat–light soaking conditions, Energy Environ. Sci. 12 (2019) 3074–3088. https://doi.org/10.1039/C9EE02043H.

[39] A.K. Jena, M. Ikegami, T. Miyasaka, Severe Morphological Deformation of Spiro-OMeTAD in (CH3NH3)PbI3 Solar Cells at High Temperature, ACS Energy Lett. 2 (2017) 1760–1761. https://doi.org/10.1021/acsenergylett.7b00582.

[40] A. Bonadio, C.A. Escanhoela, F.P. Sabino, G. Sombrio, V.G. de Paula, F.F. Ferreira, A. Janotti, G.M. Dalpian, J.A. Souza, Entropy-driven stabilization of the cubic phase of MaPbI3 at room temperature, J. Mater. Chem. A. 9 (2021) 1089–1099. https://doi.org/10.1039/D0TA10492B.

[41] M. Wang, H. Wang, W. Li, X. Hu, K. Sun, Z. Zang, Defect passivation using ultrathin PTAA layers for efficient and stable perovskite solar cells with a high fill factor and eliminated hysteresis, J. Mater. Chem. A. 7 (2019) 26421–26428. https://doi.org/10.1039/C9TA08314F.

[42] H. Tian, F. Mancilla-david, K. Ellis, P. Jenkins, E. Muljadi, A Detailed Performance Model for Photovoltaic Systems Preprint, Sol. Energy J. (2012).

[43] L. Denis, H. Grzeskowiak, D. Trias, D. Delaux, Accelerated Life Testing, in: Reliab. High-Power Mechatron. Syst. 2, Elsevier, 2017: pp. 1–56. https://doi.org/10.1016/B978-1-78548-261-8.50001-2.

[44] G. TamizhMani, J. Kuitche, Accelerated Lifetime Testing of Photovoltaic Modules Solar America Board for Codes and Standards, Sol. ABC. (2013) 106.

[45] J. You, L. Meng, T.-B. Song, T.-F. Guo, Y. (Michael) Yang, W.-H. Chang, Z. Hong, H. Chen, H. Zhou, Q. Chen, Y. Liu, N. De Marco, Y. Yang, Improved air stability of perovskite solar cells via solution-processed metal oxide transport layers, Nat. Nanotechnol. 11 (2016) 75–81. https://doi.org/10.1038/nnano.2015.230.

[46] P.S. Whitfield, N. Herron, W.E. Guise, K. Page, Y.Q. Cheng, I. Milas, M.K. Crawford, Structures, Phase Transitions and Tricritical Behavior of the Hybrid Perovskite Methyl Ammonium Lead Iodide, Sci. Rep. 6 (2016) 35685. https://doi.org/10.1038/srep35685.

[47] Q. Wang, M. Lyu, M. Zhang, J.-H. Yun, H. Chen, L. Wang, Transition from the Tetragonal to Cubic Phase of Organohalide Perovskite: The Role of Chlorine in Crystal Formation of CH3NH3PbI3 on TiO2 Substrates, J. Phys. Chem. Lett. 6 (2015) 4379–4384. https://doi.org/10.1021/acs.jpclett.5b01682.

[48] S. Wang, Y. Jiang, E.J. Juarez-Perez, L.K. Ono, Y. Qi, Accelerated degradation of methylammonium lead iodide perovskites induced by exposure to iodine vapour, Nat. Energy. 2 (2017) 16195. https://doi.org/10.1038/nenergy.2016.195.